Materials Research. 2023; 26(suppl. 1):e20220571
DOI: https://doi.org/10.1590/1980-5373-MR-2022-0571

Effect of Precipitation of Alpha Line and Sigma Phases on the Microstructure and Corrosion Resistance of the Duplex Stainless Steel SAF 2205

Isabela Dainezi[a,b,c]**, *Spyridion Haritos Borges***[a*]**, *Neide Aparecida Mariano***[a]

[a]*Universidade Federal de Alfenas, Instituto de Ciências e Tecnologia, Poços de Caldas, MG, Brasil.*
[b]*Universidade Federal de São Carlos, Departamento de Engenharia de Materiais, São Carlos, SP, Brasil.*
[c]*University of Pittsburgh, Department of Mechanical Engineering and Materials Science, Pittsburgh, PA, United States.*

Received: December 15, 2022; Revised: May 07, 2023; Accepted: May 21, 2023

The purpose of this work was to evaluate the microstructural alterations associated to the aging thermal treatments performed at 450, 475, 800 and 850°C, for 1, 3 and 12h, besides evaluating the influence of the precipitation of the alpha line phase on corrosion resistance. The samples were characterized by scanning electron microscopy, energy dispersion spectrometry, X-ray diffraction, feritscope, hardness, microhardness, in addition cyclic potentiodynamic polarization and double loop electrochemical potentiokinetic reactivation. In the agings performed at 450°C for 1h and 475°C for 12h, there was precipitation of the alpha line phase inside the ferrite and there was no significant effect on the resistance to pitting corrosion and the phenomenon of sensitization was not promoted. In the aging at 800 and 850°C for 1, 3 and 12h, the sigma phase was formed from the consumption of ferrite, and in the aging at 850°C there was the precipitation of the chi phase, promoting the increase in steel hardness. In agings for 12 h at 800 and 850°C, there was resistance to pitting corrosion decrease and the phenomenon of sensitization was moderated promoted at 800°C, with just the sigma phase precipitation and promoted at 850°C with sigma and chi phases precipitation.

Keywords: *Duplex stainless steel, Aging thermal treatment, Alpha line, Sigma, Corrosion.*

1. Introduction

Duplex stainless steels (DSS) are widely employed, especially given their performance under working conditions that require high mechanical resistance, good weldability, high corrosion resistance under tension and pitting in aqueous environments containing chloride. Nevertheless, there are restrictions associated to the working temperature, which can precipitate intermetallic phases that are hard and rich especially in chromium, leading to damages to the mechanical and corrosion properties.

The balancing of the alloying elements (Cr, Mo, Ni, Mn, N, C), associated to the processing of the alloy, promote the formation of a biphasic microstructure typical of DSS, composed of the main phases ferrite and austenite, which may be modified by the thermal treatments of solubilization and aging.

The thermal treatment of solubilization aims to promote a homogeneous microstructure composed of ferrite (α) and austenite (γ) and redissolve undesired compounds[1-9].

Cronemberger et al.[6] and Mohammed et al.[9] observed that the increase in temperature and the time of the solubilization treatment promoted a microstructure with coarse grains. In addition, they also observed that the cooling rate (slow cooling, in the furnace) influences the precipitation of intermetallic phases (sigma, chi and alpha line), and this will impact mechanical properties, such as a decrease in mechanical strength, an increase in hardness, a decrease in toughness and corrosion resistance[6,10].

The thermal treatment aging can be carried out after solubilization, to promote the precipitation of intermetallic phases, which add a set of desirable properties to the steel.

Furthermore, DSS are employed by industries such as petrochemical, chemical, nuclear and pulp and paper, that operate at high temperatures, including intervals of transformation temperature. Therefore, the aging thermal treatment is a strong ally, which allows evaluating the alterations in properties and performance the steel will present under certain service conditions, and thus avoid severe accidents when in use[10-15].

The DSS when exposed to certain temperature ranges, precipitation of intermetallic phases can occur, modifying the expected properties and become a major problem for DSS, since they can act in a deleterious way, leading to chromium depletion, and thus, directly affecting the mechanical and corrosion. These phases may be induced during welding, prolonged exposure to high temperatures and thermal treatments[15-20].

Among the possible phases to be precipitated, of harmful intermetallic phases such as secondary austenite (γ_2), alpha line (α'), sigma phase (σ), chi phase (χ), carbide and nitrides are prominent, precipitations which can occur because of the addition of alloying elements, especially chromium and molybdenum, which present a high diffusion rate and may favor this precipitation[1,15-19].

When DSS is maintained at the temperatures between 300-500°C, the diffusion of the chromium from ferrite may decompose it into a ferrite rich in Fe (α phase) and a phase rich in Cr (α' phase), and promote a phenomenon called embrittlement, with the maximum kinetics around 475°C[4,5,21-23].

*email: spyridion.hb@gmail.com

The precipitation of the α' phase introduces barriers capable of reducing the dislocation movements and, therefore, leads to an increase in yield strength, hardness, microhardness, the limit of mechanical resistance, decrease in tenacity, elongation and corrosion resistance[23-26]. Thus, the ferrite embrittled by the formation of the alpha line phase suffers a brittle cleavage-type fracture, by crack propagation at interfaces and grain boundaries, even at room temperature[26, 27].

The formation of the α' phase may occur by two mechanisms: nucleation and growth; and spinodal decomposition of ferrite, depending on the chemical composition of the DSS and the temperature to which it is exposed[23-25].

The precipitation of the α' phase by the mechanism of nucleation and growth is characterized by a greater variation in the local chemical composition, leading to the formation of nuclei of the α' phase, which grow until they reach a critical radius, promoting a barrier to nucleation[23-25].

In the mechanism by spinoidal decomposition, there is a gradual diffusion of chromium, resulting in regions rich and poor in chromium, until the phases α' (rich in chromium) and α (rich in iron) are formed as final products in the chemical compositions of equilibrium. In the spinoidal decomposition of ferrite, there is a loss in tenacity and the increase in microhardness, because of the formation of the alpha line phase, which impedes the movements of the dislocation planes[6,23-29].

Among the intermetallic phases, sigma (σ) phase is the most important because of its considerable precipitation and the negative effect on the mechanical properties and corrosion resistance[30-32]. The sigma phase precipitates between 600-900°C, preferentially in regions of high energy, because of the eutectoid reaction, in which ferrite, decomposed into sigma and secondary austenite, is nucleated in the interfaces α/γ and α/α and grows in a way to consume ferrite[26-30]. Furthermore, the sigma phase is rich in chromium and molybdenum, and thus it increases hardness and mechanical resistance, leaving DSS with lower ductility and tenacity; nevertheless, the regions adjacent to the sigma phase become depleted of chromium and molybdenum, favoring localized corrosion[33-39].

Additionally, the kinetics of the precipitation of the sigma phase reaches its maximum at 850°C, nonetheless, it is influenced by the size of the ferrite grain. The bigger the ferrite grains, the lower will be the volumetric density of grain boundaries and the higher will be the time of exposure to the temperature of transformation. In contrast, the greater the contents of chromium and molybdenum, the lower will be the time for the precipitation of the sigma phase[36-39].

The aim of this work was to analyze the influence of the aging thermal treatment performed at 450, 475, 800 and 850°C on the microstructure, microhardness and volumetric fraction of the phases, and to assess the effect of the precipitation of the alpha line phase on the resistance to localized pitting corrosion.

Due to the alpha line phase occurring at low temperatures (450-475°C) and the sigma phase at high temperatures (800-850°C), they are studied separately. So, this study aims to characterize earlier stages of these formation, as 1, 3 and 12h in terms of microstructure and microhardness changes and how it can affect the corrosion behavior.

2. Materials and Methods

The chemical composition of DSS SAF 2205 is presented in Table 1, and was obtained by inductively coupled plasma-atomic emission spectrometry (ICP-AES). Steel samples were subjected to solubilization treatment at 1100°C for 30min, followed by fast cooling in water. Subsequently, the samples were thermally treated by aging at 450, 475, 800 and 850°C, for 1, 3 and 12h, followed by cooling in water.

The samples were analyzed using an optical microscopy of the brand Carl Zeiss, model Scope A1 connected to a camera Axiocam 208 color and software ZEN Core 3.2; a scanning electron microscope (SEM), of the brand FEI, model Inspect S50, coupled to the energy-dispersive spectrometer (EDS), of the brand EDAX, model Apollo X, for the semiquantitative microanalysis of the phases, after chemical attack with Behara (2.4M HCl and 0.045M $K_2S_2O_5$).

The X-ray diffraction (XRD) analyses were performed using a diffractometer of the brand Siemens D 5005, using the Kα radiation from copper, in the range of 2θ from 40º to 100º, with a step of 0.02º for 2 s/step, and analyzed using the software Search-Match, enabling the identification of the phases.

The volumetric fraction of the ferrite phase present in each condition of the thermal treatment of aging was measured using a feritscope of the brand FISCHER model FMP30, calibrated using standards provided by the manufacturer and with the detection limit of 0.1% of ferrite. For each sample, 30 measurements were performed.

The Rockwell C hardness (HRC) measurements were performed using a Rockwell C hardness tester, of the brand Pantec Panambra, model RASN, and the measurements of Vickes microhardness (HV) were performed employing a microhardness tester of the brand Shimadzu, model HMV2, and load of 0.1 Kgf, for 15 seconds.

The techniques of cyclic potentiodynamic polarization and double cycle potentiodynamic reactivation (DL-EPR) were employed, using a potentiostat of the brand Metrohm model Autolab / PGSTAT302N, connected to an electrochemical cell composed of a saturated calomel electrode (SCE) used as reference electrode, a platinum counter electrode and the working electrode (DSS samples under the conditions of the aging thermal treatments). The electrolyte used was a solution of 3.5% of NaCl (in mass), at 25ºC, and the electrochemical measurements were performed in triplicate for each condition.

After immersion in the solution, the samples were subjected to open circuit potential (OCP) conditions, and the potentiodynamic curves were measured at a potential scan rate of 1mV/s.

Table 1. Chemical composition of DSS SAF 2205 (in % mass).

C	Mn	N	Si	Cr	Ni	Mo	Fe
0.015	1.97	0.17	0.45	23.0	5.5	3.15	bal.

The double cycle potentiodynamic reactivation (DL-EPR) technique is a device for characterizing deleterious phases, initially it was used in austenitic stainless steels, as described in the ASTM G108[40] standard. Moreover, this technique is currently extended to duplex and superduplex stainless steel. The method has been described in the ISO 12732[41] standard and has been used in the literature with several types of electrolytes and different scan rates[36,42-47].

The assays of corrosion by DL-EPR were performed in a solution composed of 1 M H_2SO_4 + 0.5 M NaCl + 0.01 M KSCN at 25°C. This choice was based on the study of Zhao et al.[43], that successfully assessed the intergranular corrosion of LDX 2404 DSS 2404 aged at 700°C. The curves by DL-EPR were obtained by the scan of the potential from -0.5 to 0.2V, and the scan was reversed and scanned from positive to negative potentials until -0.5V at a constant rate of 1.67mV/s[36, 44-48].

3. Results and Discussions

Figure 1 shows SEM micrographs of the DSS thermally treated by aging at lower magnification, that provide the general information. And in the regions indicated by circumferences micrographs were obtained at higher magnifications (Figure 2), in order to identify the presence of intermetallic phases.

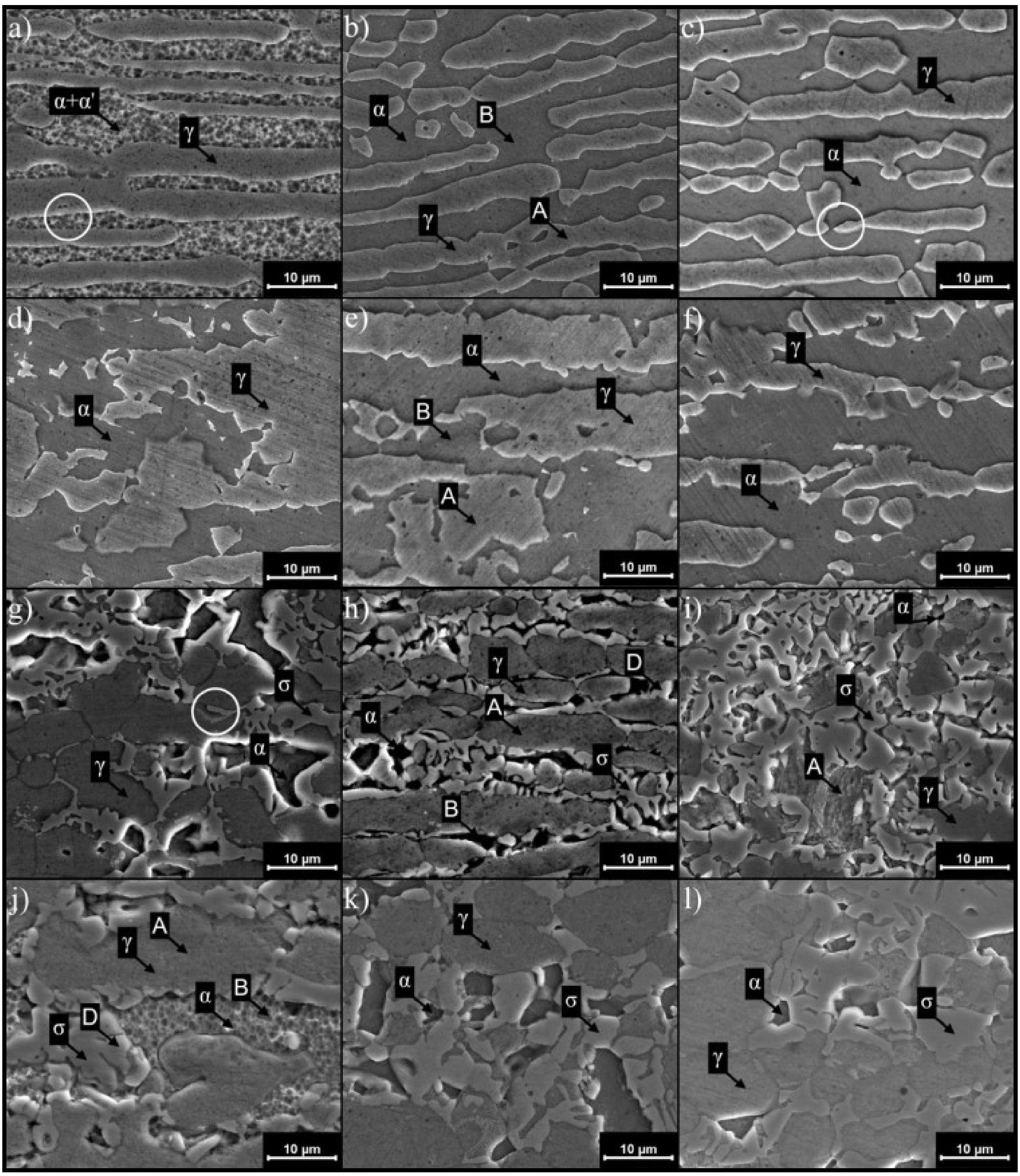

Figure 1. Micrographs of DSS SAF 2205, after thermal treatment of aging. (a-c) Aging at 450°C for 1h; 3h and 12h. (d-f) Aging at 475°C for 1h; 3h and 12h. (g-i) Aging at 800°C for 1h; 3h and 12h. (j-l) Aging at 850°C for 1h; 3h and 12h.

It was observed that aging at 450°C (Figures 1a-c and 2a) presented a microstructure composed of the austenite phase with morphology of elongated islands dispersed in the ferritic matrix; nevertheless, aging for 1h (Figures 1a and 2a) promoted the precipitation of the α' phase, inside ferrite, by the mechanism of nucleation and growth. The α' phase presents a spherical morphology with diameter around 100nm, and its formation derives from the difference in volumetric thermal expansion between the phases α and α', also observed by Li et al.[7] and Silva et al.[46]. The α' phase may cause a cross stitch, promoting a strong immobilization of the dislocation movements, and impair DSS tenacity.

In aging at 450°C for 3h (Figure 1b), only the phases ferrite and austenite were observed. And in aging at 450°C for 12h (Figures 1c and 2b), there was the precipitation of the carbides, on the boundary of the grain (α/γ), confirmed by a semiquantitative microanalysis performed by EDS, in the region indicated by C (Figure 2b), with the presence of the elements (in wt%): C (5.04), Cr (20.16), Ni (6.48), Mo (3.45) and Si (0.67).

In Figure 1d-f, it was observed that the rise in aging time at 475ºC led to an alteration in the morphology of austenite from elongated islands to grains, generating an austenite with massive structure. It happened due to the growth of austenite grains followed by their union. This process results in massive austenite and consequently in a heterogeneous microstructure[47-49].

Silva et al.[46] reported that in a sample of DSS aged at 475°C for 2000h, the formation of a phases α and α' was observed. This complex demixing process is caused by the miscibility gap between Cr and Fe, which may occur by a nucleation and growth mechanism or through spinodal decomposition, depending on the temperature, time and chemical composition, and when it occurs by spinodal decomposition the α' is dispersed so thin into α and it is possible to be detected by TEM instead of SEM[50-54].

The agings at 800 and 850°C (Figure 1g-l), regardless of time, promoted the precipitation of the σ phase; nonetheless, at 850°C, which corresponds to the maximum precipitation kinetics, it was more intense.

The precipitation of the σ phase occurs especially because of the eutectoid reactions, indicated by Equations 1 and 2[55-57]. Initially, ferrite is decomposed because of the diffusion of Cr and Mo, leaving the ferritic matrix depleted of these elements and resulting in the formation of metallic carbide ($M_{23}C_6$) and γ_2, in the ferrite/austenite interfaces, indicated by Equation 1. Subsequently, there is the transformation of ferrite in phases σ and γ_2, indicated by Equation 2, with lamellar or dissociated morphology.

$$\alpha \rightarrow M_{23}C_6 + \gamma_2 \tag{1}$$

$$\alpha \rightarrow \sigma + \gamma_2 \tag{2}$$

The formation of the sigma phase consumes Cr and Mo (ferrite stabilizers) and rejects Ni (austenite stabilizer) in the adjacent matrix, promoting the transformation of ferrite into secondary austenite[57].

In the present study, in the samples aged at 850ºC, the formation of the chi phase was observed by the transformation indicated in Equation 1, which is subsequently converted into sigma[57,58]. Furthermore, the elements Ni and Fe, at temperatures close to 800°C, are more stable in the form (Ni, Fe)x than in substitutional solution; thus, the austenite phase is more stable, with an isotropic transformation of ferrite into austenite. Additionally, the rise in aging time caused an increase in ferrite consumption and an increase in the precipitation of the sigma phase.

Under the condition of aging at 800°C for 1h, Figure 2c, there was the formation of austenite with widmanstätten morphology (Wd), nucleated, from the elongated austenite, and it grew inside the austenite grain from the grain boundary. The austenite of the Widmanstätten type grows in the form of thin, parallel platelets, an increases matrix strength, creating tensions.

From the semiquantitative microanalyses performed by EDS in regions A (phase γ), B (phase α), C (Carbides), and D (phase σ) indicated in Figures 1 and 2, it was possible to identify the corresponding phases and the chemical compositions, as shown in Table 2. The ferrite phase presents greater Cr and Mo contents, whereas the austenite phase presents a greater Ni content and the sigma phase presents high contents of Cr and Mo, since it derives from a reaction from ferrite; nevertheless, it presents differentiated morphology and properties.

Figure 3 shows the X-ray diffraction (XRD) spectra of the DSS aged at 450, 475, 800 and 850°C for 1, 3 and 12h. The agings at 450 and 475°C, performed for 1 and 12h, respectively, presented peaks referring to the α' phase, which correspond to the peaks of ferrite, but slightly shifted due to a minor alteration in network parameter (Figure 3a-b).

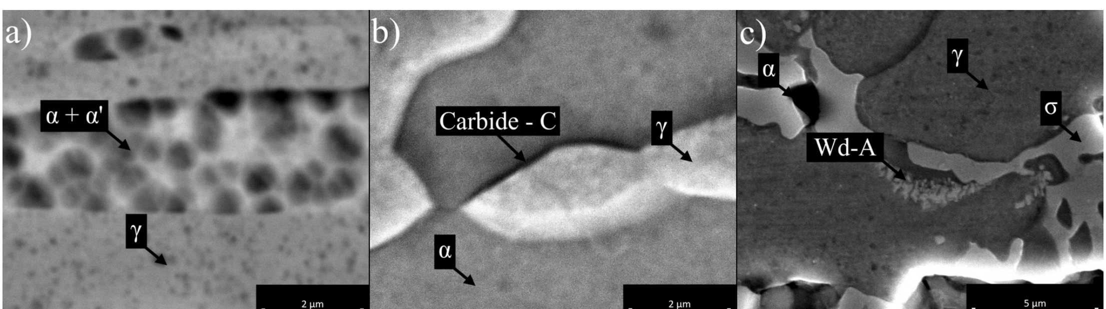

Figura 2. Detailed micrographs of DSS SAF 2205, for identification of intermetallic phases.

Moreover, the other aging times conducted at 450 and 475°C did not present significant variations and only the presence of the ferrite and austenite phases was observed, corroborating Figures 1a-f. Wang et al.[58] and Li et al.[59] observed, by XRD, after of agings performed at 400-550°C during 30min until 168h, just ferrite and austenite phases such Figure 3a-b.

Conversely, in the XRD spectra for the agings at 800 and 850°C, Figure 3c-d, respectively, the presence of the sigma phase was observed, besides the decrease in the intensity of the peaks referring to the ferrite phase, deriving from ferrite consumption for the formation of the sigma phase, corroborating Figure 1g-l.

Table 2. Results of the semiquantitative microanalyses by EDS for the aging conditions (in % mass).

Aging Temperature (°C)	Time (h)	Phase	Cr	Ni	Mo
Solubilized[24]	-	α	24.23	4.41	4.30
		γ	21.49	6.86	2.50
450	1/3/12	α	25.10	4.69	4.40
		γ	21.68	7.10	2.60
475	1/3	α	23.85	5.72	4.98
		γ	21.14	6.07	2.98
	12	α	23.15	5.13	5.41
		γ	20.36	7.05	4.00
800	1/3/12	α	27.24	5.13	1.96
		γ	21.99	6.55	2.85
		σ	27.55	3.90	5.27
850	1/3/12	α	24.22	3.96	4.84
		γ	20.23	7.07	2.54
		σ	27.27	3.41	6.25

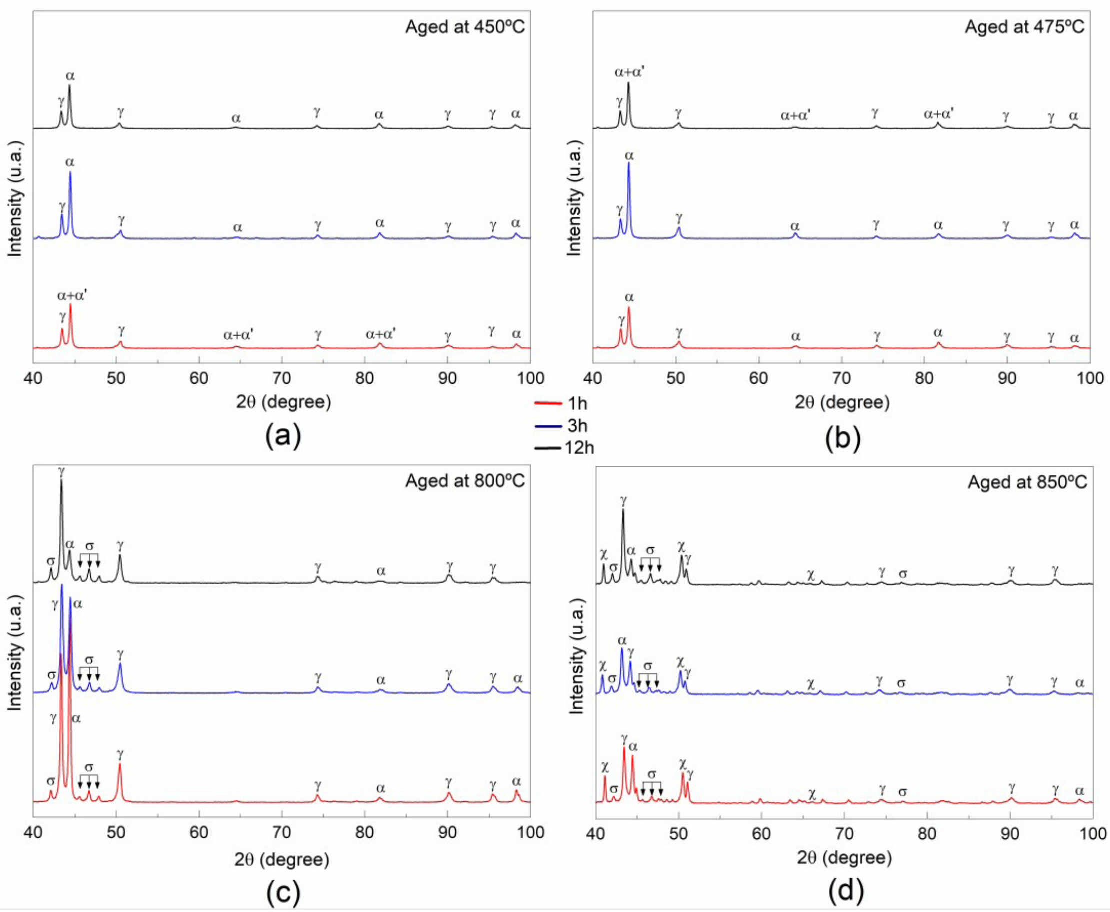

Figure 3. X-ray diffraction spectrum of the aged DSS. (a) 450°C. (b) 475°C. (c) 800°C. (d) 850°C.

Valeriano et al.[60] also observed in the aging at 850ºC a massive precipitation of the sigma phase. The χ phase precipitates preferably in ferrite/ferrite grain boundaries and before the precipitation of the σ phase[57,61].

The values of the volumetric fraction (in %v) of ferrite were obtained by feritscope testing, after the aging thermal treatments, and are presented in Table 3.

The ferrite content, which in this case represents the magnetic permeability, is to 41.39% in the solubilized condition[24] sample, decreasing throughout the times of the aging treatment, also observed by Silva[46], reductions in the magnetic permeability of DSSs during spinodal decomposition can be attributed to: the decomposition of ferromagnetic primary ferrite to paramagnetic Cr-rich α’ phase and ferromagnetic Fe-rich α phase, which leads to a decrease in the overall ferromagnetism. And the ferrite morphology resulting from spinodal decomposition, which hinders the movement of the magnetic domain walls, decreasing the magnetic permeability[61,62].

For the samples aged at 450 and 475°C, this fact derives from the increase in the austenite grains from ferrite consumption. For the samples aged at 800 and 850°C, it derives from the nucleation of the sigma phase, deriving from the decomposition of ferrite into σ and γ_2, being more intense with the rise in aging time and temperature.

The hardness values, measured after the aging thermal treatments, are presented in Table 4, where it is observed that there was no significant variation in the hardness values in the agings performed at 450 and 475°C compared to the solubilized steel (24 HRC)[24]. According to ASTM A790/A790M[63] standard, the maximum hardness of DSS is 30 HRC in the solubilized condition at 1020-1100°C followed by rapid cooling in water or moderated in air.

Nevertheless, there was a significant increase in hardness in the agings at 800 and 850°C, because of the intense reduction in the volumetric fraction of ferrite (ductile phase), besides the precipitation of the sigma phase, which presents hardening characteristics. It was also observed that the hardness values for the aging at 850°C were superior to the aging at 800ºC, given the increase in the volumetric fraction of the σ phase, besides the precipitation of the χ phase identified by X-ray diffraction.

The microhardness values (HV10) were determined in the phases (ferrite, austenite and sigma), after the aging thermal treatments, and are shown in Figure 4. Higher microhardness values of ferrite were observed under the aging conditions at 450° for 1h (308 HV10), and 475°C for 12h (302 HV10), evidencing the precipitation of the α’ phase, inside ferrite, since this phase increases microhardness because of the limitation of the dislocation movements.

The presence of the α’ phase was also observed by scanning electron microscopy (Figures 1a and 2a) under the aging condition at 450°C for 1h, being formed by the mechanism of nucleation and growth. Nevertheless, under the aging condition at 475°C for 12h, the presence of the α’ phase was identified by the increase in microhardness and by DRX, not by microscopy.

It was also observed that there was no significant variation in the microhardness values of the austenite phase, under the aging conditions at 450, 475, 800 and 850°C, in the times employed, indicating there was no formation of the G phase inside austenite.

Under aging conditions at 800 and 850°C, the microhardness of the σ phase was on averaged 670 HV10, a value also obtained by Girão[64] in DSS aged at 830°C for 60 min (680 HV10). Demonstrating the brittle character of the sigma phase and corroborating the increase in hardness of this steel under these aging conditions.

Table 3. Volumetric fraction of the ferrite phase in DSS SAF 2205.

Aging Temperature (°C)	Time (h)	Ferrite Phase (%)
Solubilized[24]	-	41.39 ± 0.96
450	1	39.06 ± 0.72
	3	37.71 ± 0.59
	12	37.58 ± 1.59
475	1	37.43 ± 0.59
	3	39.29 ± 0.38
	12	35.33 ± 1.13
800	1	16.01 ± 0.12
	3	7.47 ± 0.12
	12	2.01 ± 0.05
850	1	11.08 ± 0.15
	3	5.14 ± 0.06
	12	1.27 ± 0.05

Table 4. Hardness values of DSS SAF 2205.

Aging Temperature (°C)	Time (h)	Hardness (HRC)
Solubilized[24]	-	24 ± 1.0
450	1	21 ± 1.5
	3	21 ± 1.3
	12	23 ± 2.8
475	1	23 ± 0.4
	3	23 ± 0.9
	12	24 ± 1.8
800	1	30 ± 1.6
	3	34 ± 0.8
	12	36 ± 2.3
850	1	32 ± 1.1
	3	35 ± 0.5
	12	39 ± 0.5

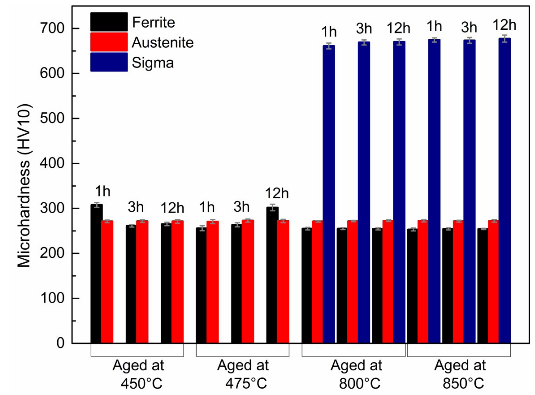

Figure 4. Microhardness values of the phases under the conditions of the aging thermal treatments.

It was also observed that there were no significant variations in the microhardness values of the ferrite and austenite phases, indicating there was no precipitation of the phases α' and G, inside ferrite and austenite, respectively.

Table 5 shows the precipitated phases under the conditions of the aging thermal treatments, and the techniques employed for their identification.

The corrosion assays by cyclic potentiodynamic polarization and double cycle potentiodynamic reactivation were performed in the samples aged at 450°C for 1h, 475°C for 12h, 800°C and 850°C for 12h, to evaluate the effect of the precipitation of the α' and sigma phases, respectively, on corrosion resistance. The samples agings at 800°C and 850°C, were used those with the longest time (12h), because of the most critical condition to sigma precipitation.

Figures 5a and 5b show the open circuit potential (OCP) and cyclic potentiodynamic polarization curves, respectively, in a 3.5 wt% sodium chloride solution at room temperature. The values of the corrosion potentials (E_{corr}) were obtained from curve of the Figure 5a, as shown in Table 6.

It was verified that the evolution of the open circuit potential is shifted to positive values with time, characterizing the formation of a passive layer[4,20], stable and adherent to the steel surface, and the potentials stayed stable from 1800s of immersion.

The scan of potential in the cyclic potentiodynamic polarization started at more negative potentials than the corrosion potential, causing a partial removal of the passivation layer. Thus, it was observed that the corrosion potential (E_{corr}) was greater for the open circuit potential than in the cyclic potentiodynamic polarization.

Figure 5b demonstrates that the cyclic potentiodynamic polarization curves are positive hysteresis, in other words, current density in reverse scanning is greater than in the direction of advancement of the current densities.

A clear formation of a current density plateau is observed in a broad potential range. This current density establishes steel passivity, identified as passivation current density (I_{pass}), by the formation of a passive film, with a protective characteristic, of good adherence and good stability, promoting a reduction in corrosion speed. The aging at 450°C for 1h and 475°C for 12h presented two distinct passive regions are observed, given the duplex microstructure of DSS, composed of the ferrite and austenite phases. This region is not observed under conditions for 12 h at 800 and 850°C, due to the low % ferrite.

Table 5. Precipitated phases under the conditions employed in the aging treatment.

Aging Temperature (°C)	Time (h)	Phase/Technique
450	1	α (MEV/EDS/DRX)
		γ (MEV/EDS/DRX)
		α' (MEV/DRX/Microhardness)
450	3	α (MEV/EDS/DRX)
		γ (MEV/EDS/DRX)
450	12	α (MEV/EDS/DRX)
		γ (MEV/EDS/DRX)
		C (MEV/EDS)
475	1	α (MEV/EDS/DRX)
		γ (MEV/EDS/DRX)
475	3	α (MEV/EDS/DRX)
		γ (MEV/EDS/DRX)
475	12	α (MEV/EDS/DRX)
		γ (MEV/EDS/DRX)
		α' (DRX/Microhardness)
800	1	α, γ, σ (MEV/EDS/DRX)
		Wd (MEV)
800	3/12	α, γ, σ (MEV/EDS/DRX)
850	1/3/12	α, γ, σ (MEV/EDS/DRX)
		χ (DRX)

Table 6. Open circuit potential of the DSS in a 3.5% NaCl solution.

AID SAF 2205	Ecorr (mV)
Aged at 450°C/1h	-131 ± 3
Aged at 475°C/12h	-123 ± 5
Aged at 800°C/12h	-152 ± 24
Aged at 850°C/12h	-185 ± 1

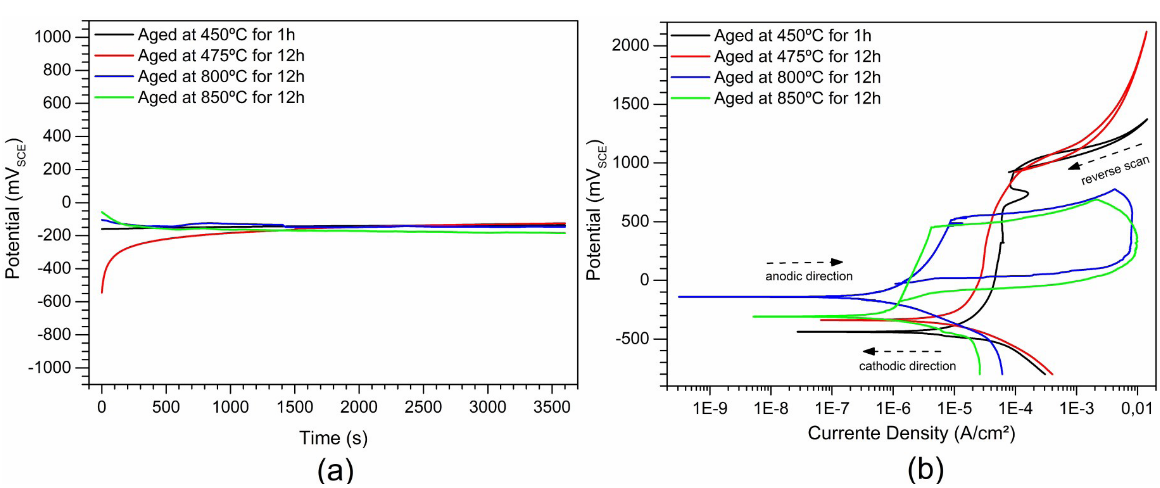

Figure 5. Corrosion assay in a 3.5% NaCl solution. (a) Evolution of the open circuit potential. (b) Cyclic potentiodynamic polarization.

These phases present distinct contents of the elements chromium and molybdenum, which act as stabilizers and passivators in the ferrite phase, whereas in the austenite phase they only promote passivation. Thus, the ferrite phase suffers passivation more rapidly than the austenite phase, being associated to the first passive region of the polarization curve, and the second passive region is associated to the passivation of the austenite phase. From the polarization curves in Figure 5b, the electrochemical parameters were obtained, as shown in Table 7.

According to Dainezi[25], DSS, under the condition solubilized at 1100°C for 30min and cooled in water, presented a corrosion current density of 10.2×10^{-6} A/cm^2, in 3.5% of NaCl at room temperature. Comparing this result with the values obtained for the steel aged at 450°C for 1h and 475°C for 12h, it is observed that there were no significant variations, indicating the corrosion rate is similar under these conditions; therefore, alpha line precipitation inside ferrite was not capable of altering corrosion rate.

The polarization curve of the aging condition at 475°C/12h is shifted to lower current densities ($I_{pass}=1.9 \times 10^{-5}$ A/cm^2), in comparison with the aging condition at 450°C/1h ($I_{pass}=6.0 \times 10^{-5}$ A/cm^2), a fact which suggests that the precipitation of the α' phase by spinoidal decomposition, finely dispersed inside ferrite, promoted the formation of the passive film more rapidly than by nucleation and growth.

The passivation current density (Ipass), for the conditions of aging for 12h at 800°C and 850°C, were 2.8×10^{-6} A/cm^2 and 3.4×10^{-6} A/cm^2, respectively, indicating that the formation of the passive film occurred more quickly in the conditions 800°C and 850°C, but at the level of passivation current density, in a lower potential range.

The presence of the chlorine ions adsorbed on the surface of the steel increases the number of active sites, responsible for the localized rupture of the passive film, and starts pit nucleation and growth. Thus, pit potential (E_{pit}) is the potential above which the pits are nucleated and develop and, as a consequence, there is a sharp increase in current density, indicating the beginning of the pit does not depend only on the property of the film, but also on the oxide/solution interface.

Under the condition aged at 450°C/1h, oscillations in the anode current density were observed at potentials below the pit potential, referring to the nucleation and repassivation of metastable pits, because of the presence of the α' phase finely dispersed inside ferrite. When the pit potential is reached, these metastable pits become stable, and grow preferably on the boundaries of the α/α and α/γ grains, and inside the austenite grains, characterizing a selective corrosion. Nevertheless, in of aging for 12 at 800°C 850, a reduction in the values of pit and protection potential was observed, because of the precipitation of phase sigma (σ) and promoting the formation of regions poor in chromium, and consequently, reducing corrosion resistance. The pits were identified as hemispherical (Pit-H) and irregular (Pit-I), as shown in Figure 6.

Table 7. Electrochemical parameters of DSS in a 3.5% NaCl solution.

AID SAF 2205	E_{corr} (mV)	I_{corr} (A/cm^2)	E_{pit} (mV)	E_{prot} (mV)	I_{pass} (A/cm^2)	$\Delta E_p = E_{pit} - E_{corr}$ (mV)
Aged at 450°C/1h	-380±8	(8.4±3.1) x10^{-6}	1004±7	999±8	(6.0±3.0) x10^{-5}	1384
Aged at 475°C/12h	-339±7	(9.8±1.2) x10^{-6}	1008±2	945±11	(1.9±0.2) x10^{-5}	1347
Aged at 800°C/12h	-234±47	(2.2±0.8) x10^{-7}	651±57	-51±13	(2.8±0.9) x10^{-6}	768
Aged at 850°C/12h	-272±32	(1.3±0.4) x10^{-7}	404±54	-196±18	(3.4±0.5) x10^{-6}	676

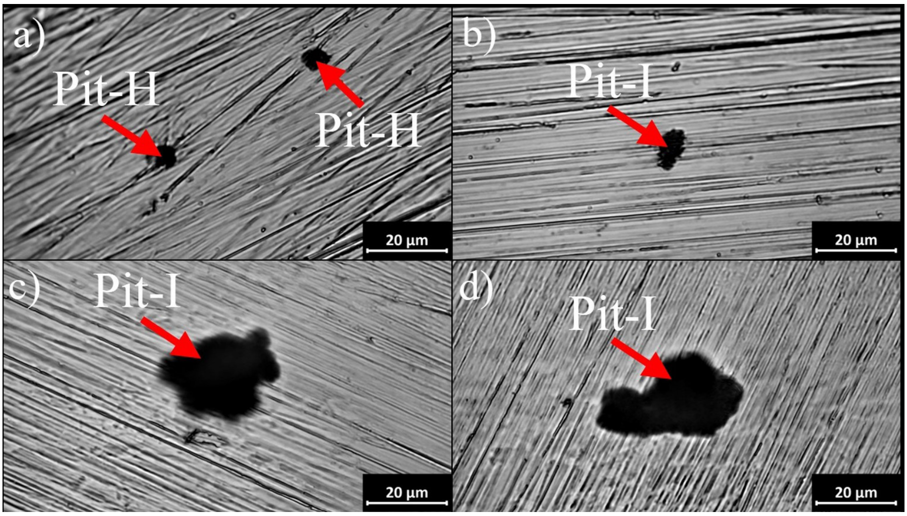

Figure 6. Micrographs obtained by optical microscopy after the assay of corrosion by potentiodynamic polarization of the aged DSS. (a) 450°C/1h. (b) 475°C/12h. (c) 800°C/12h. (d) 850°C/12h.

The resistance to pitting corrosion can be related to the passive condition on the steel surface, by the difference between the pit and corrosion potentials, given by the relation: $\Delta E_p = (E_{pit} - E_{corr})$. The aging conditions at 450°C/1h and 475°C/12h presented the values of 1384mV and 1347mV, respectively, and a similar value was obtained by Dainezi et al.[24] for the DSS aged at 500°C for 1h (ΔE_p=1452mV), indicating the precipitation of the α' phase did not present a significant effect on pit corrosion resistance. Li et al.[10] also evidenced that the precipitation of the α' phase did not lead to the reduction in corrosion resistance.

The protection potential (E_{prot}) was determined in the potential where the polarization curve is intercepted after the reversion in scanning. It is defined as the potential below which the already existing pits will be passivated and there is no nucleation of new pits. The aging condition at 450°C/1h presented a higher E_{prot} (999mV), compared to the aging at 475°C/12h (E_{prot}=945mV); therefore, it presents a greater ease in the repassivation of the formed pits.

Nevertheless, in of aging for 12h at 800 and 850ºC, a reduction in the values of pit and protection potential was observed, because of the precipitation of phase sigma (σ) and promoting the formation of regions poor in chromium, and consequently, reducing corrosion resistance.

Figures 7a and 7b show the curves of the open circuit potential (OCP) and of the double cycle potentiodynamic reactivation, respectively, in a solution composed of 1 M H_2SO_4 + 0.5 M NaCl + 0.01 M KSCN at 25°C.

In Figure 7a, it is observed that the aging condition at 450°C/1h presented a decrease in the potentials over time and subsequently, the potential remained constant, characterizing a generalized corrosion, followed by the formation of the passive layer. On the other hand, for the aging condition at 475°C/12h, the values of the potentials are approximately constant over time, indicating the formation of a stable and adherent passive layer on the surface of the steel. The values of the corrosion potentials (E_{corr}) were obtained from the curves in Figure 7a, as shown in Table 8.

The double loop electrochemical potentiokinetic reactivation (DL-EPR), consists of polarizing the steel with a constant scan rate towards the anodic direction, ranging from the open circuit potential to the passive region. Then, the scan is reversed towards the open circuit potential with the same scan rate.

During the anodic polarization, the current reaches its maximum to a known value, the activation current density (Ia). On the reverse scan, the passive film formed during the anodic polarization is expected to degrade, firstly, on the weaker areas around the deleterious phases. Therefore, another current peak is formed, the reactivation current density (Ir). The ratio Ir/Ia is proportional to the degree of deleterious phases (degree of Sensitization) present[41].

All conditions had peaks of reactivation after the reversion of the scanning direction. The reactivation during the reversion of the scan is associated with the breakdown of the passive film in the regions where the depletion of Cr and Mo, due to the formation of deleterious phases.

It can be observed in Figure 7b that there is an evidente increase in Ia and Ir for the sample aged 12h at 800 and 850°C. This increase may be related to the development of chromium and molybdenum depleted areas due to the intermetallic phase formation.

The curves of double cycle potentiodynamic reactivation of the DSS under the conditions aged at 450°C/1h and 475°C/12h (Figure 7b), show the presence of two peaks in the activation current, because of the biphasic microstructure of DSS. The resulting curve represents the sum of the curves of the existing phases. The peak of the highest potential corresponds to austenite (peak 1), and the peak of the smallest potential (peak 2) corresponds to the ferrite phase.

Table 8. Open circuit potential in a solution of 1M H_2SO_4 + 0.5M NaCl + 0.01M KSCN.

AID SAF 2205	E_{corr} (mV)
Aged at 450°C/1h	-417 ± 2
Aged at 475°C/12h	-419 ± 1
Aged at 800°C/12h	-404 ± 2
Aged at 850°C/12h	-409 ± 1

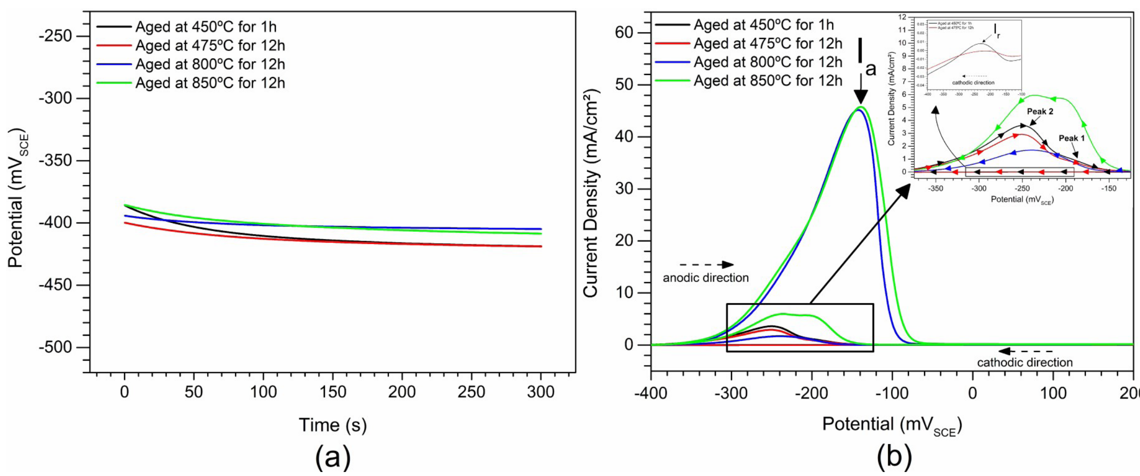

Figure 7. Corrosion assay in a solution of 1M H_2SO_4 + 0.5M NaCl + 0.01M KSCN. (a) Evolution of the open circuit potential. (b) double loop electrochemical potentiokinetic reactivation.

Table 9. Degree of sensitization of the DSS in a solution of 1M H_2SO_4 + 0.5M NaCl + 0.01M KSCN.

AID SAF 2205	Ia (mA/cm^2)	Ir (mA/cm^2)	Degree of Sensitization (Ir/Ia)
Aged at 450°C/1h	3.54 ± 0.40	0.0053 ± 0.0010	0.0015 ± 0.0004
Aged at 475°C/12h	3.13 ± 0.30	0.0032 ± 0.0008	0.0010 ± 0.0008
Aged at 800°C/12h	39.60 ± 4.00	1.2300 ± 0.3000	0.0304 ± 0.0050
Aged at 850°C/12h	44.90 ± 1.30	5.4300 ± 0.4000	0.1210 ± 0.0080

However, the samples aged 12h at 800 and 850°C (Figure 7b), the presence of these two peaks is not observed due to the low fraction of the ferrite phase compared to austenite, and presented a bigger current density peak compared to 450°C/1h and 475 °C/12h, due to the presence of the sigma phase, which causes chromium depletion in adjacent regions, leading to a decrease in corrosion resistance.

By the DL-EPR curves, the sample aged at 450ºC for 1h presented a bigger current density peak than the sample aged at 475°C for 12h, indicating this condition requires a higher critical current density for its passivation. This derives from the more intense formation of regions poor in chromium, caused by the precipitation of the α' phase, by the mechanism of nucleation and growth.

According to Silva et al.[46], it is expected that the regions adjacent to the precipitate α' be depleted in chromium in the early stages of the formation of the α' phase, whereas by the mechanism of spinoidal decomposition, chromium-depleted areas are gradually formed and the impact on corrosion resistance only becomes severe after a large period of time. Thus, the impact at the initial stages is more evident with the formation of α' by the mechanism of nucleation and growth, corroborating the greater degree of sensitization under this condition.

Moreover, the peak Ir for the sample aged at 800°C for 12h (1.23 mA/cm^2) is smaller than the peak Ir for that sample aged at 850°C for 12h (5.43 mA/cm^2), indicating that chromium-depleted zones in 850°C for 12h condition are more present[65].

According to ISO 12732/2006[41], degree of sensitization (Ir/Ia) with lower values than 0.01 mean that the material is not sensitized. Morever, values between 0.01 and 0.05 mean a moderate sensitization and values bigger than 0.05 mean that the material is sensitized. The Table 9 shows the degree of sensitization obtained from the curves of DL-EPR.

For the lowest temperature conditions (450 and 475°C) was observed that under both aging conditions, the degree of sensitization was inferior to 0.01 (Table 9), characterizing the absence of the sensitization phenomenon[38,39]; furthermore, it indicates there was no rupture of the passive layer. Therefore, in agings at 450/1h and 475°C/12h, despite the precipitation of the deleterious phase α', there was no sensitization, and thus the depletion of Cr and Mo was insignificant.

The sample at aged for 12 h at 800°C had the sensitization degree (0.03) value between 0.01 and 0.05, therefore a moderate sensitization, while the sample aged for 12 h at 850°C had the sensitization degree (0.12) value bigger than 0.05, therefore is sensitized. Due to the sigma phase is a deleterious phase, rich in Cr and Mo, the matrix became impoverished in Cr and Mo, thus corrosion behavior is worse. Moreover, the sample aged for 12h at 850°C also has χ phase which means more depletion in Mo in the ferrite and in the grain boundary α/γ[66], so the corrosion behavior is worse then samples with just sigma phase precipitated, like that one aged at 800°C for 12h.

4. Conclusion

The precipitation of the α' phase was observed only in the aging treatments performed at 450°C for 1h and 475°C for 12h. Its formation occurred, respectively, by the mechanisms of nucleation and growth, and spinoidal decomposition of ferrite, and it resulted in:

- High values for the microhardness of the ferrite phase because of the limitation of the dislocation movements caused by α' nucleation;
- The precipitation of the α' phase did not have a significant effect on the pitting corrosion resistance, and it did not promote the sensitization phenomenon.

Under the aging conditions at 800 and 850°C for 1, 3 and 12h, there was the formation of the sigma phase from ferrite consumption. Additionally:

- In the aging at 850°C there was the precipitation of the chi phase, which is subsequently consumed for the formation of the sigma phase;
- Under the aging conditions at 800 and 850°C, the microhardness of the sigma phase was around 670 HV10, demonstrating the embrittling character of the phase and corroborating the increase in steel hardness under these aging conditions.
- The precipitation of the σ phase decreases the pitting corrosion resistance and the σ phase with χ phase together promoted the sensitization phenomenon (850°C for 12h).

5. Acknowledgements

The authors thank the Brazilian research funding agencies FAPEMIG, FAPESP, CNPq, FINEP and CAPES for the financial support.

6. References

1. Breda M, Pezzato L, Pizzo M, Calliari I. Effect of cold rolling on pitting resistance in duplex stainless steels. Metall Ital. 2014;6:15-9.
2. Gennari C, Lago M, Bögre B, Meszaros I, Calliari I, Pezzato L. Microstructural and Corrosion properties of cold rolled laser welded UNS S32750 Duplex Stainless Steel. Metals (Basel). 2018;8(12):1074. http://dx.doi.org/10.3390/met8121074.
3. Gonçalves FJF, Martins M. Tecnologia dos materiais. Araranguá: Cefet/SC; 2008.
4. Alvares-Armas I, Degallaix-Moreuli S. Duplex stainless steels. Londres: ISTE Ltd and John Wiley&Sons; 2009.

5. Cronemberger MER, Mariano NA, Coelho MFC, Pereira JN, Ramos ÉCT, de Mendonça R, et al. Study of cooling rate influence on SAF 2205 duplex stainless steel solution annealed. Mater Sci Forum. 2014;802:398-403. http://dx.doi.org/10.4028/www.scientific.net/MSF.802.398.
6. Cronemberger MER, Nakamatsu S, Rovere CAD, Kuri SE, Mariano NA. Effect of cooling rate on the corrosion behavior of as-cast SAF 2205 duplex stainless steel after solution annealing treatment. Mater Res. 18(Suppl 2):138-42.
7. Rezende SC, Dainezi I, Apolinario RC, Sousa LL, Mariano NA. Influence of molybdenum on solution-treated and on the corrosion by pite of duplex stainless steel in solution of lithium chloride. Mater Res. 2019;22(Suppl 1):e20190138.
8. Rezende SC, Cronemberger MER, Silva R, Della Rovere CA, Kuri SE, Sousa LL, Mariano NA. Effect of solution annealing time on the microstructure and corrosion resistence of duplex stainless steel. Mater Sci Forum. 2018;390:374-9.
9. Mohammed AM, Shrikrishna KA, Sathiya P. Effects of post weld heat treatment on friction welded duplex stainless steel joints. J Manuf Process. 2016;21:196-200.
10. Li X, Lo KH, Kwok CT, Sun YF, Lai KK. Post-fire mechanical and corrosion properties of duplex stainless steel: comparison with ordinary reinforcing-bar steel. Constr Build Mater. 2018;174:150-8. http://dx.doi.org/10.1016/j.conbuildmat.2018.04.110.
11. Jinlong LV, Tongxiang L, Chen W, Limin D. Comparison of corrosion properties of passive films formed on coarse grained and ultrafine-grained AISI 2205 duplex stainless steels. J Electroanal Chem. 2015;757:263-9.
12. Kisasoz A, Gurel S, Karaaslan A. Effect of annealing time and cooling rate on precipitation processes in a duplex corrosion-resistant steel. Metal Sci Heat Treat. 2016;57:544-7. http://dx.doi.org/10.1007/s11041-016-9919-5.
13. Gowthamana PS, Jeyakumara S, Saravanan BA. Machinability and tool wear mechanism of duplex stainless steel: a review. Mater Today Proc. 2020;26(Pt 2):1423-9. http://dx.doi.org/10.1016/j.matpr.2020.02.295.
14. Papula S, Song M, Pateras A, Chen XB, Brandt M, Easton M, et al. Selective laser melting of duplex stainless steel 2205: effect of post-processing heat treatment on microstructure, mechanical properties, and corrosion resistance. Materials (Basel). 2019;12(15):2468. http://dx.doi.org/10.3390/ma12152468. PMid:31382506.
15. Murkut P, Pasebani S, Isgor OB. Effects of heat treatment and applied stresses on the corrosion performance of additively manufactured super duplex stainless steel clads. Materialia (Oxf). 2020;14:100878. http://dx.doi.org/10.1016/j.mtla.2020.100878.
16. Pezzato L, Lago M, Brunelli K, Breda M, Calliari I. Effect of the heat treatment on the corrosion resistance of duplex stainless steels. J Mater Eng Perform. 2018;27:3859-68. http://dx.doi.org/10.1007/s11665-018-3408-5.
17. Zhang Y, Cheng F, Wu S. Improvement of pitting corrosion resistance of wire arc additive manufactured duplex stainless steel through post-manufacturing heat-treatment. Mater Charact. 2021;171:110743. http://dx.doi.org/10.1016/j.matchar.2020.110743.
18. Prabhu P, Rajnish G. Effect of Intermetallic phases on corrosion behavior and mechanical properties of duplex stainless steel and super-duplex stainless steel. Adv Sci Technol Res J. 2015;9:87-105. http://dx.doi.org/10.12913/22998624/59090.
19. Putz A, Hosseini VA, Westin EM, Enzinger N. Microstructure investigation of duplex stainless steel welds using arc heat treatment technique. Weld World. 2020;64:1135-47. http://dx.doi.org/10.1007/s40194-020-00906-2.
20. Shariq A, Hättestrand M, Nilsson JO, Gregori A. Direct observation on quantification of nanoscale decomposition in super duplex stainless steel weld metals. J Nanosci Nanotechonol. 2009;9(6):3657-64.
21. Hosseini VA, Thuvander M, Wessman S, Karlsson L. Spinodal decomposition in functionally graded super duplex stainless steel and weld metal. Metall Mater Trans, A Phys Metall Mater Sci. 2018;49:2803-16. http://dx.doi.org/10.1007/s11661-018-4600-9.
22. Cícero S, Setién J, Gorrochategui I. Assessment of termal aging embrittlement in a cast stainless steel valve and its effect on the structural integrity. Nucl Eng Des. 2009;239(1):16-22.
23. Gunn RN. Duplex stainless steels - microstructure, properties and applications. Cambridge: Abington Publishing; 2003.
24. Dainezi I, Borges SH, Souza LL, Mariano NA. Temperature and time effect of thermal aging treatment on microstructure and corrosion resistance of UNS S31803 duplex stainless steel. Res Soc Dev. 2021;10(8):e24910817369.
25. Dainezi I. Efeito do tratamento térmico de envelhecimento na microestrutura e na resistência à corrosão do aço inoxidável duplex [dissertação]. Poços de Caldas: Universidade Federal de Alfenas; 2019.
26. Chen Y, Yang B, Zhou Y, Wu Y, Zhu H. Evaluation of pitting corrosion in duplex stainless steel Fe20Cr9Ni for nuclear power application. Acta Mater. 2020;197:172-83. http://dx.doi.org/10.1016/j.actamat.2020.07.046.
27. Sahu JK, Krupp U, Ghosh RN, Christ H-J. Effect of 475°C embrittlement on the mechanical properties of duplex stainless steel. Mater Sci Eng A. 2009;508(1-2):1-14. http://dx.doi.org/10.1016/j.msea.2009.01.039.
28. Liu X, Lu W, Zhang X. Reconstructing the decomposed ferrite phase to achieve toughness regeneration in a duplex stainless steel. Acta Mater. 2020;183:51-63. http://dx.doi.org/10.1016/j.actamat.2019.11.008.
29. Wang R. Precipitation of sigma phase in duplex stainless steel and recent development on its detection by electrochemical potentiokinetic reactivation: a review. Corros Comm. 2021;2:41-54.
30. Hosseini VA, Karlsson L, Wessman S, Fuertes N. Effect of sigma phase morphology on the degradation of properties in a super duplex stainless steel. Materials (Basel). 2018;11:933. http://dx.doi.org/10.3390/ma11060933. PMid:29865160.
31. Iacoviello F, Di Cocco V, D'Agostino L. Integranular corrosion susceptibility analysis in austeno-ferritic (duplex) stainless steels. Fatigue Fract Eng Mater Struct. 2017;3:276-82.
32. Mampuya MB, Umba MC, Mutombo K, Olubambi PA. Effect of heat treatment on the microstructure of duplex stainless steel 2205. Mater Today Proc. 2021;38(Pt 2):1107-12. http://dx.doi.org/10.1016/j.matpr.2020.06.196.
33. Silva DDS, Sobrinho JMB, Souto CR, Gomes RM. Application of electromechanical impedance technique in the monitoring of sigma phase embrittlement in duplex stainless steel. Mater Sci Eng A. 2020;788:139457. http://dx.doi.org/10.1016/j.msea.2020.139457.
34. Biezma MV, Martin U, Linhardt P, Ress J, Rodríguez C, Bastidas DM. Non-destructive techniques for the detection of sigma phase in duplex stainless steel: a comprehensive review. Eng Fail Anal. 2021;122:105227. http://dx.doi.org/10.1016/j.engfailanal.2021.105227.
35. Silva R, Kugelmeier CL, Vacchi GS, Martins CB, Dainezi I, Afonso CRM, et al. A comprehensive study of the pitting corrosion mechanism of lean duplex stainless steel grade 2404 aged at 475 °C. Corros Sci. 2021;191:109738. http://dx.doi.org/10.1016/j.corsci.2021.109738.
36. Hosseini VA, Karlsson L, Wessman S, Fuertes N. Effect of sigma phase morphology on the degradation of properties in a super duplex stainless steel. Materials (Basel). 2018;11(6):933. http://dx.doi.org/10.3390/ma11060933. PMid:29865160.
37. Abra-Arzola JL, García-Rentería MA, Cruz-Hernández VL, García-Guerra J, Martínez-Landeros VH, Falcón-Franco LA, et al. Study of the effect of sigma phase precipitation on the sliding wear and corrosion behaviour of duplex stainless steel AISI 2205. Wear. 2018;400:43-51. http://dx.doi.org/10.1016/j.wear.2017.12.019.

38. Inácio LKP, Wolf W, Leucas BCB, Stumpf GC, Santos DB. Microtexture evolution of sigma phase in an aged fine-grained 2205 duplex stainless steel. Mater Charact. 2021;171:110802.
39. Gunn RN. Duplex stainless steels: microstructure, properties and applications Cambridge, England: Abington Publishing; 1997. http://dx.doi.org/10.1533/9781845698775.
40. ASTM: American Society for Testing and Materials. ASTM G108-94: standard test method for electrochemical reactivation (EPR) for detecting sensitization of AISI Type 304 and 304L stainless steels. West Conshohocken: ASTM; 2010.
41. ISO: International Organization for Standardization. ISO/TC 156. ISO 12732:2006: corrosion of metals and alloys — electrochemical potentiokinetic reactivation measurement using the double loop method (based on Cihal's method). Geneva: ISO; 2006.
42. Lo KH, Kwok CT, Chan WK. Characterisation of duplex stainless steel subjected to long-term annealing in the sigma phase formation temperature range by the DLEPR test. Corros Sci. 2011;53(11):3697-703. http://dx.doi.org/10.1016/j.corsci.2011.07.013.
43. Zhao H, Zhang Z, Zhang H, Hu J, Li J. Effect of aging time on intergranular corrosion behavior of a newly developed LDX 2404 lean duplex stainless steel. J Alloys Compd. 2016;672:147-54.
44. Wu TF, Tsai W-T. Effect of KSCN and its reactivation behavior of sensitized alloy 600 in sulfuric acid solution. Corros Sci. 2003;45(2):267-80. http://dx.doi.org/10.1016/S0010-938X(02)00100-2.
45. Assis KS, Sousa FVV, Miranda M, Margarit-Mattos ICP, Vivier V, Mattos OR. Assessment of electrochemical methods used on corrosion of superduplex stainless steel. Corros Sci. 2012;59:71-80.
46. Silva R, Baroni LFS, Kugelmeier CL, Silva MBR, Kuri SE, Rovere CAD. Thermal aging at 475°C of newly developed lean duplex stainless steel 2404: mechanical properties and corrosion behavior. Corros Sci. 2017;116:66-73. http://dx.doi.org/10.1016/j.corsci.2016.12.014.
47. Hilders OA, Zambrano N, Ochoa JLM. Microstructural evolution and mechanical property-fractal behavior relations of na aged super duplex stainless steel. Acta Microscopica. 2018;27(2):83-107.
48. Elsabbagh FM, Hamouda RM, Taha MA. On microstructure and microhardness of isothermally aged UNS S32760 and the effect on toughness and corrosion behavior. J Mater Eng Perform. 2013;23:275-84.
49. Melo EB, Magnabosco R, Moura C No. Influence of the microstructure on the degree of sensitization of a Duplex Stainless Steel UNS S31803 aged at 650°C. Mater Res. 2013;16(6):1336-43.
50. Chan KW, Tjong SC. Effect of secondary phase precipitation on the corrosionbehavior of duplex stainless steels. Materials (Basel). 2014;7(7):5268-304. http://dx.doi.org/10.3390/ma7075268. PMid:28788129.
51. Shi SK, Yan J, Zhang Y, Wang Y, Wang J. The microstructure evolution of 2205 stainless steel in long-term aging at 500◦C. Nucl Eng Des. 2012;250:167-72. http://dx.doi.org/10.1016/j.nucengdes.2012.05.030.
52. Krupp U, Söker M, Giertler A, Dönges B, Christ H-J, Wackermann K, et al. The potential of spinodal ferrite decomposition for increasing the very high cycle fatigue strength of duplex stainless steel. Int J Fatigue. 2016;93:363-71. http://dx.doi.org/10.1016/j.ijfatigue.2016.05.012.
53. Westraadt JE, Olivier EJ, Neethling JH, Hedström P, Odqvist J, Xu X, et al. A high-resolution analytical scanning transmission electronmicroscopy study of the early stages of spinodal decomposition in binary Fe–Cr. Mater Charact. 2015;109:216-21.
54. Wan J, Ruan H, Wang J, Shi S. The kinetic diagram of sigma phase and its precipitation ardening effect on 15Cr-2Ni duplex stainless steel. Mater Sci Eng A. 2018;711:571-8.
55. Li JS, Cheng G-J, Yen H-W, Wu LT, Yang Y-L, Wu RT, et al. Thermal cycling induced stress–assisted sigma phase formation in super duplex stainless steel. Mater Des. 2019;182:108003. http://dx.doi.org/10.1016/j.matdes.2019.108003.
56. Kashiwar A, Vennela NP, Kamath SL, Khatirkar RK. Effect of solution annealing temperature on precipitation in 2205 duplex stainless steel. Mater Charact. 2012;74:55-63. http://dx.doi.org/10.1016/j.matchar.2012.09.008.
57. Escriba DM, Materna-Morris E, Plaut RL, Padilha AF. Intermetallic phase precipitation in duplex stainless steels during high temperature exposition. Mater Sci Forum. 2010;636:478-84. http://dx.doi.org/10.4028/www.scientific.net/MSF.636-637.478.
58. Wang S, Ma Q, Li Y. Characterization of microstructure, mechanical properties and corrosion resistance of dissimilar welded joint between 2205 duplex stainless steel and 16MnR. Mater Des. 2011;32(2):831-7.
59. Li X, Lo KH, Kwok CT, Sun YF, Lai KK. Post-fire mechanical and corrosion properties of duplex stainless steel: comparison with ordinary reinforcing-bar steel. Constr Build Mater. 2018;174:150-8. http://dx.doi.org/10.1016/j.conbuildmat.2018.04.110.
60. Valeriano LC, Correa EO, Mariano NA, Robin ALM, Machado MAGTC. Influence of the solution-treatment temperature and short aging times on the electrochemical corrosion behaviour of Uns S32520 Super Duplex Stainless Steel. Mater Res. 2019;22(4):22. http://dx.doi.org/10.1590/1980-5373-2018-0774.
61. Pardal JM, Tavares SSM, Fonseca MC, de Souza JA, Côrte RRA, de Abreu HFG. Influence of the grain size on deleterious phase precipitation in superduplex stainless steel UNS S32750. Mater Charact. 2009;60(3):165-72. http://dx.doi.org/10.1016/j.matchar.2008.08.007.
62. Lo KH, Lai JKL. Microstructural characterisation and change in a.c. magneticsusceptibility of duplex stainless steel during spinodal decomposition. J Nucl Mater. 2011;401(1-3):143-8.
63. ASTM: American Society for Testing and Materials. ASTM A790/A790M: standard specification for seamless and welded ferritic/austenitic stainless steel pipe. West Conshohocken: ASTM; 2022.
64. Girão DC. Influência da fase sigma na resistência à corrosão do aço inoxidável super duplex ASTM A890 grau 1C após tratamento isotérmico [dissertação]. Fortaleza: Centro de Tecnologia, Universidade Federal do Ceará; 2015.
65. Badji R, Bouabdallah M, Bacroix B, Kahloun C, Bettahar K, Kherrouba N. Effect of solution treatment temperature on the precipitation kinetic of σ-phase in 2205 duplex stainless steel welds. Mater Sci Eng A. 2008;496(1-2):447-54. http://dx.doi.org/10.1016/j.msea.2008.06.024.
66. Higa SM. Avaliação da resistência à corrosão e das propriedades mecânicas da junta soldada de aço inoxidável duplex [dissertação]. São Carlos: Universidade Federal de São Carlos; 2015.